Monte Carlo Simulations of Colloidal Pair Potential Induced by Telechelic Polymers: Statistics of Loops and Bridges

Vincent Testard, Julian Oberdisse,* and Christian Ligoure

Laboratoire des Colloïdes, Verres et Nanomatériaux, UMR 5587 CNRS/UM2, Université Montpellier II, F-34095 Montpellier Cedex 5, France

Received March 17, 2008; Revised Manuscript Received July 3, 2008

ABSTRACT: A Monte Carlo study of the statistics of loop and bridge formation between colloidal particles, and in particular micelles, by telechelic polymers is presented. The experimental fact that the hydrophobic outer blocks of a triblock copolymer tend to stick into micelles in aqueous solution is mimicked by counting only polymer chains with both ends on the surface of the micelles. The long inner hydrophilic block is generated by a random walk procedure. It is excluded from the volume of the micelles, and it can form either a loop, with both stickers on the same micelle, or a bridge, with the stickers on two different micelles. In this paper, the pair potential is determined between two micelles as a function of distance and chain-to-micelle size ratio, for ideal and self-avoiding chains. In the latter case, the effect of many chains has also been explored.

1. Introduction

Self-assembling networks are common in both natural and synthetic materials. They consist of self-assembled aggregates (nodes) that are reversibly connected by links with a finite lifetime as opposed to chemical gels where junctions are permanent. These physical gels exhibit two universal and independent features: a thermodynamic first-order phase separation, which occurs at a low volume fraction between a dilute and concentrated solution even in the absence of any specific interaction, and a nonthermodynamic topological transition, where an infinite network spanning the entire volume of the system is formed.[1] Telechelic polymers are often used as model linkers because they are architecturally simple: they consist of a long solvophilic midblock with each end terminated by a solvophobic short chain (a sticker). The stickers incorporate into the solvophobic domains of the aggregates and can bridge them via their solvent-soluble midblock, resulting in an attractive interaction between the aggregates. The nature and morphologies of the aggregates forming the network are versatile: (i) telechelic polymers in binary solution[2] that self-assemble spontaneously into noninteracting flowerlike micelles at low concentrations and form three-dimensional networks above a threshold concentration,[3] (ii) surfactant vesicles,[4,5] (iii) lyotropic lamellar phases,[6,7] (iv) wormlike micelles,[8−10] (v) spherical micelles,[7,11] and (vi) oil-in-water[12,13] or water-in-oil[14] microemulsion droplets. This last system (telechelic/microemulsion mixtures) is of particular fundamental interest. Indeed, the advantage of this system is that the parameters that control the thermodynamics and structure of the physical gel can be easily identified and independently controlled: the concentration of nodes (the droplets) and the number of polymers per droplet. This is in contrast with binary mixtures of telechelics, where the number of nodes formed by the associating chain ends cannot be controlled separately. Other advantages of this system are the spherical symmetry which allows, for instance, a simple structural analysis in the Fourier space from scattering experiments and the versatility of the control of the surface curvature.

Because of the high solvophobic energy ($\approx 10-20 k_B T$), the chain ends are constrained to lie within the droplets and the number of dangling chains outside the droplets is statistically insignificant. Nevertheless, the stickers can detach from a droplet and switch between loops (with both ends inside the same droplet) and bridges (with the chain ends residing in different droplets). Stickers can also be exchanged between the droplets during droplet collisions. Phase behavior, structural properties on one hand, and elasticity in the gel region on the other hand will be controlled by the distribution of loops and bridges between the aggregates[15] and will depend on several parameters: the concentrations of droplets and linkers as well as the sizes of polymers and droplets.

Modeling such a complicated self-assembly is a formidable challenge, because of the wide range of scales involved. Different complementary theoretical approaches to describing these reversible gels have been proposed. The mean field analytical model developed by Zilman et al.[16] allows for a generic qualitative prediction of the phase diagram of microemulsions with telechelic linkers: it predicts that the system undergoes a robust first-order phase separation into a dense highly connected phase in equilibrium with dilute droplets decorated by polymer loops as the number of polymers per drop is increased, despite the absence of any specific interaction between either the droplets or the polymer chains. On the other hand, a hybrid Monte Carlo/molecular dynamics numerical approach by Hurtado et al.[17] coarse grains the polymer description and retains their effect only as links inducing a phenomenological entropic interaction between the two droplets they connect. This model predicts the same type of phase diagram but also a gelation line determined by geometric percolation unrelated to phase separation, as observed experimentally by Filali et al.[14] It also allows the investigation of the gel dynamics, which is outside the scope of this paper.

A quantitative description of the interactions induced by telechelic polymers between droplets needs a polymeric approach that can predict the loop and bridge distribution as a function of the various relevant parameters, i.e., the mean droplet separation, the mean number of stickers per droplet, the droplet-to-polymer size ratio, and the quality of the solvent. Such an approach could be also useful for the quantitative analysis of the scattering experiments performed with these systems.[14,18−20] The first theoretical approach was proposed by Milner and Witten, who adapted self-consistent field calculations to telechelic polymer brushes between flat plates.[21] These authors found a weak attractive minimum in the free energy near a separation close to brush contact due to the increased entropy per bridge in the contact. This calculation was revisited by Meng

* To whom correspondence should be addressed. E-mail: oberdisse@lcvn.univ-montp2.fr.

10.1021/ma8005813 CCC: $40.75
Published on Web 09/19/2008

and Russel,[22] who obtained a stronger attraction between the plates in better agreement with experimental results.[23,24] Results similar to those of Milner and Witten were obtained by Bjorling and Stilbs,[25] who examined the good solvent case numerically using a Scheutjens−Fleer approach. The corresponding problem with curved surfaces is considerably more difficult, and Semenov et al. have proposed a scaling approach.[26] To the best of our knowledge, the only results for potentials published on telechelic chains linking surfaces with a finite curvature are from Bhatia and Russel.[27] These authors calculated equilibrium configurations of telechelic ideal polymer chains between flat plates and curved surfaces using a diffusion-equation approach[28] and obtained analytical results for flat plates and numerical results for chains between two spheres. They obtained several interesting results. A fairly strong attractive minimum in the free energy on the order of $O(k_BT)$ occurs at separations slightly inferior to the end-to-end distance of the free chain. The attraction increases as the chain-to-sphere size ratio increases. The authors anticipated, however, several limitations to their approach. The repulsive interaction due to the confinement of the attached chains is strongly underestimated due to the deflection of the chains out of the gap at close separations. Second, many chain effects which become relevant for real chains cannot be investigated by this approach and should certainly also modify the relative distribution of loops and bridges, as well as the total number of allowed chain configurations especially at close separation. Porte et al.[18] used a model derived by Bhatia and Russel[27] to analyze the experimental small angle neutron scattering spectra of microemulsion droplets linked by telechelic polymers. Despite a fairly good semiquantitative agreement between the theory and the experiments, they have determined that the repulsive part of the polymer-induced interaction between the spheres was not properly described by the current theoretical models. This observation was the principal motivation for revisiting theoretically the interaction induced by telechelic polymers between spheres. We choose a Monte Carlo simulation approach to analyze step by step the different parameters that control the polymer configurations, to extract a realistic interaction potential between the spheres from a microscopic description.

The paper is organized as follows. In section 2, the statistical mechanics of the problem is presented, linking the number of configurations to the interaction potential between particles. Note that we have chosen to use the simplest possible model, based on a constantly renewed lattice generation of chains, excluding all Monte Carlo sampling around a given chain configuration (cf. ref 29 for a recent review). In section 3, results are discussed. As a reference case, we start with the chain configurations on a single particle. Subsequently, the configurations of ideal and real chains between particles are presented as a function of chain-to-particle size ratio and surface-to-surface distance between particles and converted to a pair interaction potential. To finish, the impact of the number of chains between two particles on the pair potential is discussed for self-avoiding chains.

2. Model and Methods

2.1. Partition Function and Pair Potential. We consider two impenetrable spheres of radius R, representing each a micelle or colloid, at a surface-to-surface distance h, in interaction with Q chains which consist each of $N_{seg} \gg 1$ freely jointed linear segments (termed "monomers") of length b. We denote R_g the radius of gyration of a chain, and we assume that there is no interaction between the spheres and the chains except with the chain ends that prefer to be adsorbed on a sphere: the corresponding sticking energy (energy difference of a sticker in the solvent and a sticker adsorbed on the sphere) is denoted by ε. There are four possible states for a chain: free chains (f) with no sticker adsorbed on a sphere, dangling chains (d) with a single sticker adsorbed on a sphere, loops (l) with both stickers of the chain on the same sphere, and finally bridges (b) where the two stickers of the chain are adsorbed on the two spheres and link them. For aqueous transient networks, the stickers consist of short chains of typically 10−25 methylene groups, with a sticking energy on the order of kT per methylene group. Therefore, the corresponding sticking energy is $\varepsilon/kT \approx 10-25$, large enough to neglect the fraction of dangling or free chains. The partition function of the Q chains then reads

$$Z_Q(h,R) = \sum_{\text{configurations}} e^{-E/kT} = \Omega_b + \Omega_l + \Omega_d e^{-\epsilon/kT} + \Omega_f e^{-2\epsilon/kT} \approx \Omega_b + \Omega_l \quad (1)$$

where Ω_i is the number of configurations of chains in state i.

For ideal chains, the partition function of Q chains is related to the partition function of a single chain z_{ideal} through

$$Z_{Q,ideal}(R,h) = \frac{[z_{ideal}(R,h)]^Q}{Q!} = \frac{(\Omega_{1,b} + \Omega_{1,l})^Q}{Q!} \quad (2)$$

where $\Omega_{1,b}$ ($\Omega_{1,l}$) is the number of bridge (loop) configurations of a single chain.

To estimate the two contributions to the partition function (eq 1), for a given (Q,R,h) macrostate we will generate a large number of sample configurations using a Monte Carlo approach. For a sufficiently large number of runs, the following proportionality rule is satisfied

$$\frac{\Omega_l + \Omega_b}{\Omega_{tot}} = \frac{N_l + N_b}{N_{tot}} \quad (3)$$

where Ω_{tot} (N_{tot}) is the total number of configurations (generation attempts, i.e., the number of generated configurations). In our calculation, chains always start from one sphere (no free chains), and Ω_{tot} includes thus loops, bridges, and failures. "Failures" are dangling chains or chains which collide with the spheres during their construction or violate the excluded volume condition for self-avoiding chains. For the calculation of the potential, it is important to realize that with this definition Ω_{tot} is independent of the distance between the particles.

The effective interparticle pair potential induced by Q polymer chains is given by the difference in the free energy of the telechelic chains for two spheres at distance h and for two isolated spheres:

$$U_Q(h,R) = -k_BT[\ln Z_Q(R,h) - \ln Z_Q(R,\infty)] \quad (4)$$

From eqs 1 and 3, with $\Omega_{Q,b}(h\to\infty,R) = 0$, and keeping in mind that Ω_{tot} is independent of h, we obtain

$$U_Q(h,R) = -kT\left\{\ln\left[\frac{N_b(R,h) + N_l(R,h)}{N_{tot}(R,h)}\right] - \ln\left(\frac{N_l^\infty}{N_{tot}^\infty}\right)\right\} \quad (5)$$

where N_l^∞ (N_{tot}^∞) is the number of loops (generation attempts) obtained for a distance between the sphere larger than the maximum extension of the chains.

Notice that for ideal chains, the effective interaction pair potential is additive; i.e., $U_Q(h,R) = QU_1(h,R)$, where $U_1(h,R)$ is the effective pair potential induced by a single chain. In the case of self-avoiding ("real") chains, the partition function of the total system, including all chains, needs to be calculated.

2.2. Details of Monte Carlo Chain Generation. The aim of the Monte Carlo algorithm is to generate statistically independent chains of N_{seg} segments, representing monomers or groups of monomers, of unity length each ($b = 1$). Depending on the desired chain statistics, we generate either ideal chains, i.e., without any correlations between segments positioned on a lattice, or self-avoiding chains.

Lattice Generation of Chains. Chains are generated on a cubic lattice with a lattice constant set to unity. Segments are added in a stepwise process starting from an initiator segment by choosing among the six directions in space with equal probability. Naturally,

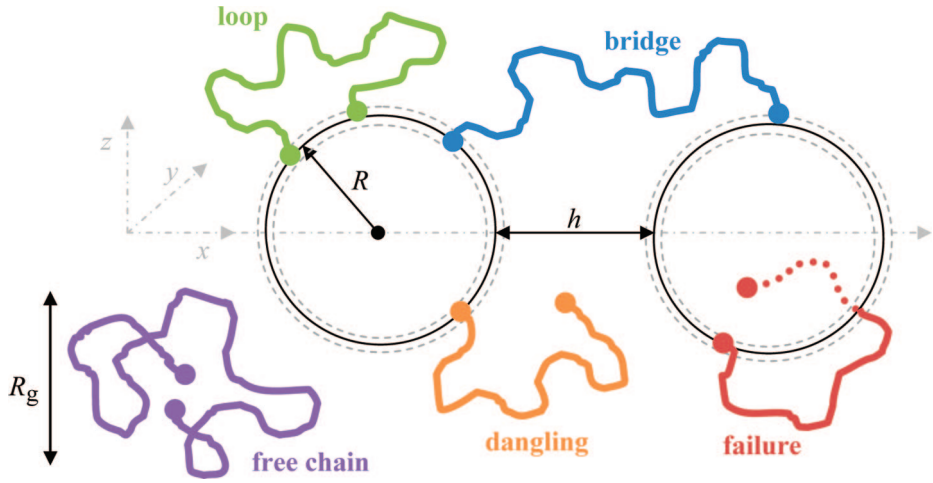

Figure 1. Illustration of chain generation results. Chains can either form loops or bridges, have a dangling end, or produce a chain generation failure by hitting a bead. Bridges or loops are present if the last monomer is placed in a thin shell with a thickness equal to one segment length *b*. Radius *R* and interbead distances *h* will be given in reduced units (α and *β*, respectively), which are normalized to the radius of gyration of a free chain.

this leads to ideal chain statistics (cf. Appendix). In the case of excluded volume interactions, a return to the previous lattice node is excluded, as well as double occupancy of any lattice node. In the case of violation of excluded volume, the entire chain is discarded and a new chain is started to avoid undesired correlations. In the Appendix, it is also shown that such chains obey the well-known excluded volume statistics. In this article, we refer to chains generated according to this procedure as real chains. We have also checked that lattice and off-lattice simulations of ideal chains give identical results.

System of Two Interacting Beads. To determine the pair potential between colloidal beads as a function of distance and for different bead diameters, we define the following reduced variables. The radius of gyration of the free polymer chain, R_g^{free}, is used as a basis. The radius of the beads, *R*, is then expressed as

$$\alpha = \frac{R}{R_g^{free}} \tag{6}$$

and the surface-to-surface distance *h* is written

$$\beta = \frac{h}{R_g^{free}} \tag{7}$$

This situation is depicted in Figure 1.

Boundary Conditions of Telechelic Stickers. Chains in simulations with one or two colloidal beads start on the surface of one bead and may end either on the same bead (loop), on the second bead (bridge), or in free space (dangling end). As discussed in section 2.1, we count the number of times each situation occurs in determining the pair potential. The first segment representing the sticker starts on the surface of any bead. To recognize loops and bridges, we have defined a shell with a thickness of unity (one segment) centered on the surface of each bead. This is illustrated in Figure 1. If the last segment of the chain hits this shell, the second polymer sticker is assumed to be linked to this bead. All beads are considered impenetrable in this simulation, with the exception of the shell used for the last segment. In all other cases, if any segment of a chain hits a bead, the entire chain is discarded.

Observables. Common observables of chains are the end-to-end vector ($\mathbf{R}_e$) and the radius of gyration of a chain (R_g)[30] which both characterize the average spatial extent of the chains. We have also used a tensor of the components of the end-to-end vector ($\mathbf{T} = \langle \mathbf{R}_e \mathbf{R}_e \rangle$) which is a convenient way to detect anisotropy of the coil, e.g., of a chain attached to large sphere. The spatial distribution of segments (or monomers) between beads, $\Phi(\mathbf{r})$, has been determined by averaging over many chains and according to the cylindrical symmetry, yielding $\Phi(x,z)$. We have estimated the error bars of

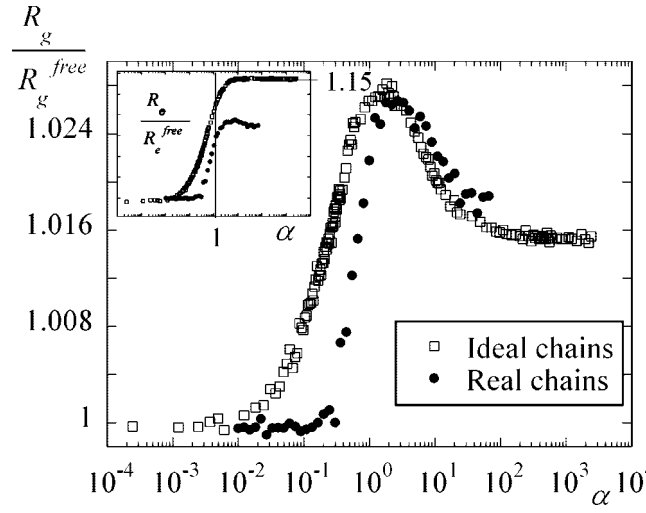

Figure 2. Ratio of the radius of gyration of grafted chains and free ones as a function of reduced bead radius α for ideal (10^5 chains; $N_{seg} = 10^4$) and excluded volume chains (2×10^5 chains; $N_{seg} = 100$). In the inset, the end-to-end vector for the same parameters is shown.

the number of successful bridges ($N_{bridges}$) and loops (N_{loops}) as well as dangling ends (N_{dang}) by performing a certain number of runs (N_{run}, typically several hundred for ideal chains and tens for real chains, each run consisting of 20000 successful chain generations) and determining the average and standard deviation of the distribution of results. These averages are used to deduce the potential, with error bars corresponding to a 90% confidence interval of the potential determined from the standard deviations of $N_{bridges}$ and N_{loops}.

3. Results and Discussion

3.1. Single Chain Grafted on a Bead. As a simple reference case, we have simulated the conformation of a single chain grafted on a bead. This allows us to study the perturbation of the chain caused by the presence of an impermeable bead. Ideal and excluded volume chain statistics on beads of various radii (α from 0.01 to 200 for real chains, up to 10^4 for ideal ones) have been determined and are reported in terms of the radius of gyration in Figure 2.

The low-α limit in Figure 2 corresponds to grafting on extremely small spheres, and naturally, the radius of gyration of free chains is recovered. In the other limiting case ($\alpha \gg 1$),

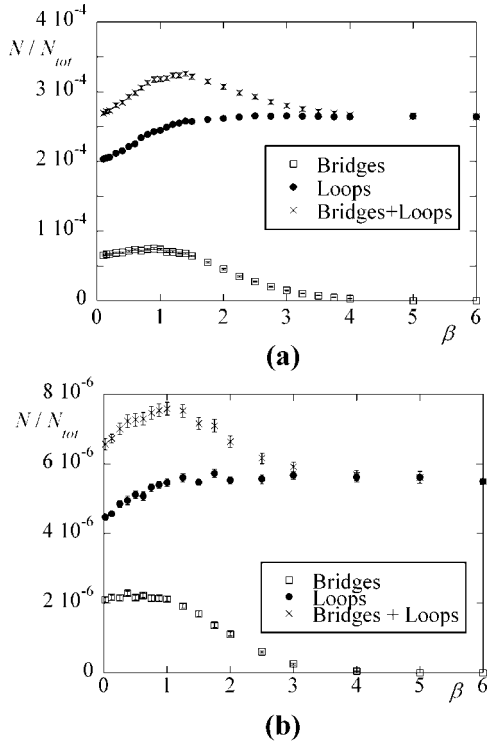

Figure 3. Fractions of bridges and loops among all chains (including failures and dangling ends) (a) for ideal chains ($\alpha = 1$, $N_{seg} = 200$, 2×10^4 chains per run, $N_{run} = 800$) as a function of reduced surface-to-surface distance ($\beta = 0.01-6$) and (b) for excluded volume chains ($\alpha = 1$, $N_{seg} = 100$, 2×10^4 chains per run, $N_{run} = 10$) as a function of β varying from 0.01 to 6.

the conformation of a chain grafted to a flat surface is found. Both limiting cases also validate our simulation method, as these cases have been determined independently. In particular, all other observables, like the end-to-end tensor, or the ratio of R_g to R_e, agree. In the intermediate region, a somewhat large transient is observed. It has a peculiar maximum, at different locations for ideal and real chains, which we think is due to geometrical constraints, which to the best of our knowledge has not been reported in the literature. It may also be noted that the height of the maximum is only a few percent, i.e., the effect is weak, the coil being simply displaced from the surface. The effect is much stronger for the average end-to-end distance (the ratio increases by ~15% between low and high α values), shown as the inset in Figure 2, which can be explained by the fact that one end is fixed on the bead, in some sense on the "surface" of the coil. This stronger effect apparently masks the small maximum, which is not observed for the end-to-end distance of ideal chains, and hardly for real chains.

3.2. Single Chain between Two Beads. We now turn to the simulation of chain configurations between two beads as depicted in Figure 1. As a first result, the fraction of bridges and loops among all completed chains is plotted in panels a (ideal) and b (real chains) of Figure 3, as well as the sum of both which is needed as input for the potential. As one can see from these results, the fraction of successful loop and bridge generation is rather low ($\approx 10^{-4}$) for ideal chains; nonetheless, the statistics are very satisfying, and a clear shape emerges in Figure 3a. For real chains, the probability of success decreases to $\approx 10^{-6}$, and the statistics become worse due to the longer running times, leading to significantly fewer runs. However, also in this case, the general tendency is evident from Figure 3b. We can clearly see two regimes in Figure 3: At short distances ($\beta \leq 1$), the number of bridges and loops increases, whereas at higher values, the number of loops levels off while

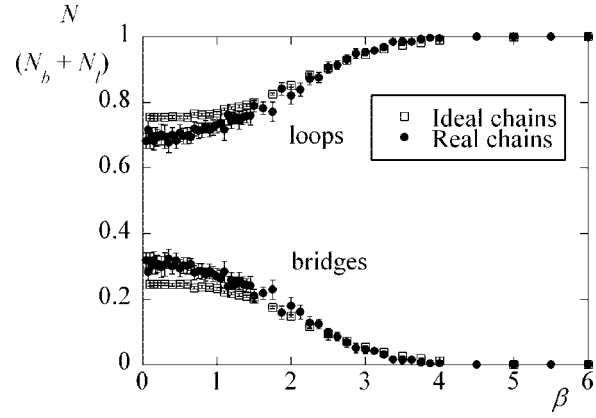

Figure 4. Fraction of bridges and loops among all chains contributing to the interaction potential (without failures and dangling ends) for ideal chains ($\alpha = 1$, $N_{seg} = 200$, 2×10^4 chains per run, $N_{run} = 800$) and for excluded volume chains ($\alpha = 1$, $N_{seg} = 100$, 2×10^4 chains per run, $N_{run} = 10$) as a function of β varying from 0.01 to 6.

the number of bridges decreases to zero after having reached a maximum close to $\beta = 1$. This behavior dictates the shape of the potential and in particular the close range interaction: Increasing numbers of bridges and loops correspond to a decreasing potential as a function of distance. Thus, the potential is short-range repulsive only if the sum of bridges and loops at $\beta = 0$ is less than the number of loops at large distances. Finally, the maximum position in the number loops and bridges corresponds to the position of the potential minimum.

In Figure 4, the same information is represented as a fraction of bridges and loops among all completed chains with the second sticker on a bead. In other words, loops and bridges add up to 100% in this plot. This representation evidences thus the ratio of bridges to loops and can be directly used to evaluate contributions to the rheological properties of networks of beads bridged by a polymer. This result has been used recently to interpret the rather low shear modulus observed in networks, approximately one-third of what one would expect from simple network theory ($G = \nu kT$), which is due to the lower number of rheologically active links (bridges) with respect to the total amount of polymer.[19] Note that the fraction of bridges varies between 20 and 30% for interparticle distances typically encountered in our experiments with microemulsion networks (it is set by the concentration of particles), and this numerical agreement is encouraging. With regard to the range of the interaction, it is clear from Figure 4 that there are no bridges and only loops at large interparticle distances, that bridges start to build up around $\beta \approx 3$, and are established in their majority at distances comparable to the average end-to-end distance of polymers ($\beta \approx 2$). Results for real and ideal chains are quite similar, with slightly more bridges at close contact for excluded volume chains. Error bars are, of course, considerably larger in this latter case.

A different way to visualize the polymer conformations is to plot the monomer density, taking advantage of the cylindrical symmetry of the two-particle problem, and average over toric regions equidistant from the two particles. In Figure 5, the monomer density is plotted for a given particle size ($\alpha = 0.5$, ideal chains) and for two different distances ($\beta = 0.1$ on the left and $\beta = 1.5$ on the right). The three rows correspond to monomers being part of bridges only (top), those being part of loops only (middle), and all monomers (bottom). The monomer density is found to be concentrated around the particle, clearly in the form of loops, for isolated particles (large β), whereas the monomer density between the beads increases as the beads approach. Monomer density plots calculated for other choices of parameters are presented as Supporting Information.

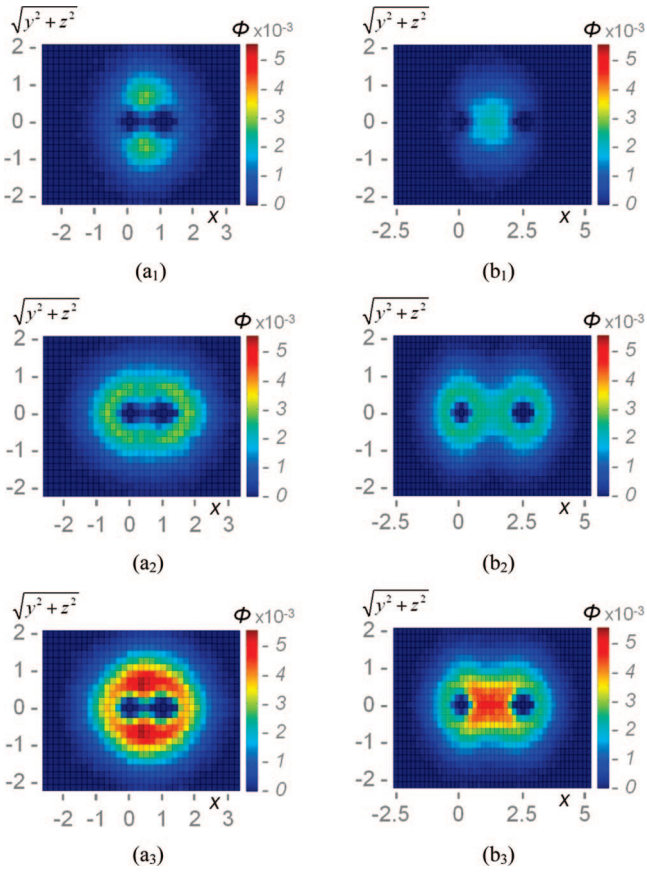

Figure 5. Average monomer density $\Phi(x,z)$ of chains having both stickers attached to a bead ($\alpha = 0.5$): (1) bridges only, (2) loops only, and (3) bridges and loops. These quantities have been computed for interparticle distances (a) $\beta = 0.1$ and (b) $\beta = 1.5$. $\Phi(x,z)$ is normalized such that its integral over all monomers equals one for each reduced surface-to-surface distance β. x and $z = (y^2 + z^2)^{1/2}$ are also expressed in reduced units.

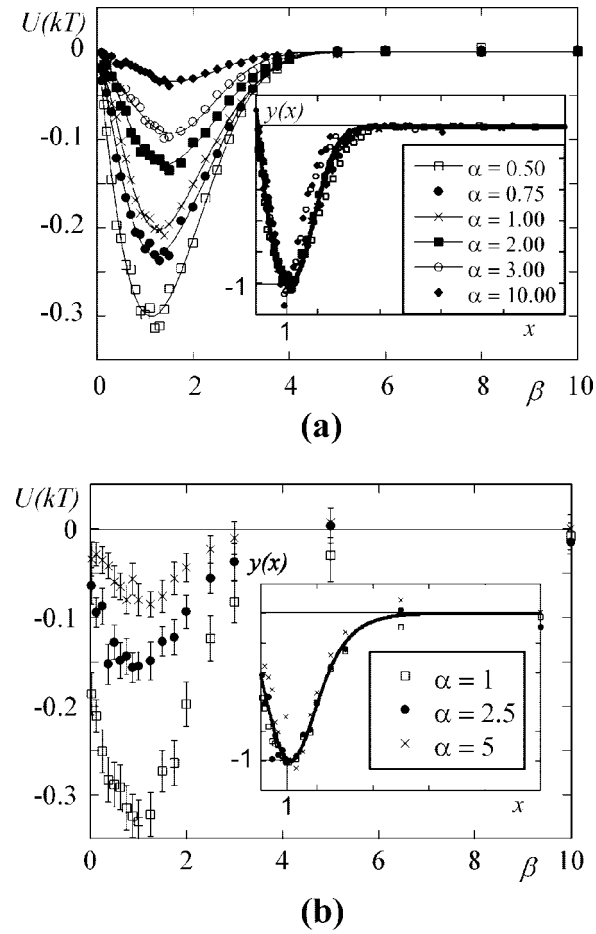

Figure 6. (a) Pair potential induced by one ideal chain between two particles as a function of reduced surface-to-surface distance β (from 0.01 to 10), for different particle radii ($\alpha = 0.5-10$, $N_{seg} = 200$, 2×10^4 chains per run, $N_{run} = 800$). (b) Same quantities for one excluded volume chain ($\alpha = 1$, 2.5, and 5; $N_{seg} = 100$, 2×10^4 chains per run, $N_{run} = 10$). Corresponding master curves are shown in the inset of each panel, where $x = \beta/\beta_{min}$ and $y = U/U_{min}$. Their characteristics (β_{min} and U_{min}) are given in the Appendix.

As outlined in section 2, the statistics of bridges and loops can be used to calculate the potential induced between the particles by the chains (cf. eq 5). Two families of potentials are plotted in Figure 6, for ideal and self-avoiding chains, for different particle radii. In Figure 6a, the strong influence of bead size on the potential induced by ideal chains is evidenced: the larger the particles with respect to the polymer, the shallower the potential. For the smallest particles, the minimum of the potential reaches ~0.3 kT and is located at $\beta = 1.13$ ($\alpha = 0.5$, ideal chains). At larger distances, the potential approaches zero quite quickly and is clearly negligible at $\beta > 4$. At small surface-to-surface distances, the potential goes to zero as well. The other curves, obtained for different particle sizes (α), look very similar, apart from a slight shift of the minimum to a higher β, and of course a reduction in depth. This similarity suggests plotting the potentials shown in Figure 6a in a reduced representation, fixing the minimum position and depth to 1. This superposition is shown to work reasonably well in the inset of Figure 6a, where minor deviations concerning the range of the reduced potentials, decreasing with α, are observed. An empirical fit to this master curve, the equation of which is given in the Appendix, is also shown in the inset. The evolution of the potential with the sphere-to-polymer size ratio suggests that for an identical sphere-to-polymer molar ratio, a larger modulus should be measured for longer polymer chains. We also predict that the phase diagram should be affected: The binodal line should shift to smaller Q values for longer polymer chains, which corresponds to a more efficient bridging interaction.

In the case of a single real chain between two beads, the error bars on the fractions of bridges and loops (Figure 4) are considerably larger due to the lower success probability in chain generation. Nonetheless, a minimum located around $\beta = 1$, followed by a slow increase to zero for $\beta > 3$ or 4, is clearly visible. The minimum at 0.33 kT for $\alpha = 1$ is approximately five-thirds of its value for ideal chains (0.2 kT for $\alpha = 1$), and unlike with ideal chains, the potential stays negative up to contact between beads ($\beta = 0$).

Both with ideal and with real chains, the potential is found to show no short-range repulsion. At first sight, this is surprising, as one would expect the chains not to like to be compressed between the particles, thereby reducing their entropy. What happens can be understood when we return to Figure 5, where the bridges are seen to be expelled from the gap between the particles as they approach. As a cross-check, we have made test calculations with a first sticker fixed at the point closest to the second bead, and we have shown that there is then a strongly repulsive interaction for both ideal and real chains. This means that the polymer molecules oppose less resistance to the approach of the particles if they can escape laterally. This effect is due to our description in terms of pairs of particles, which neglects particles and polymer surrounding any other particle in solution. In a real system, polymer bridges between all surrounding beads occupy volume and reduce the degrees of freedom of a given molecule. In other words, many-particle

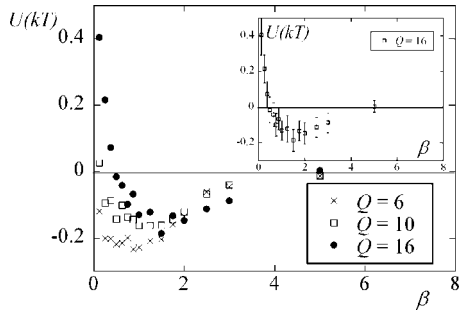

Figure 7. Interaction potential between two colloidal particles ($\alpha = 1$) induced by 6, 10, and 16 polymer chains, with excluded volume interactions, as a function of reduced surface-to-surface distance β. In the inset, the pair potential for $Q = 16$ chains is plotted with error bars.

contributions to the interaction potential may exist. We expect them to be less important in the case of many chains with excluded volume between a pair of particles, as then the chains can not all escape from the gap between the particles, due to repulsive interactions with the other chains. This extension of our model will be discussed in the next paragraph.

3.3. Many Excluded-Volume Chains between Two Beads. The pair potential obtained by one real chain between two beads is shown in Figure 6b, and we have noticed the absence of short-range repulsion. As mentioned in the preceding paragraph, we have therefore extended our simulations to multichain situations, varying the number of real chains between two beads from 1 to 16. In the case of ideal chains, the potential is of course simply proportional to the number of (noninteracting) chains.

Due to difficulties with the long simulation times of real chains, we generate a first chain as described before. Additional chains are created one by one in presence of the ones already completed, until the desired number is obtained. When a chain hits any obstacle during its polymerization, just this last chain (and not all previously completed ones, as would be necessary to obtain completely unbiaised chain statistics) is discarded and entirely reconstructed. For excluded-volume chains, the increase in chain number and thus monomer density around a particle reduces the volume accessible to a given chain (note that the radius of gyration of the chains is equal to the radius of the particles for $\alpha = 1$). This limits the squeezing out of chains from the gap between particles and thus induces a rapid growth of the number of loops and bridges as β increases from zero. From eq 5, this results in a short-range repulsion, as shown in Figure 7. For a single chain, the potential stays below zero at low β, and the value of $U(0)$ increases with the number of chains. The position of the minimum shifts to higher β values with chain number. This effect can be explained by the increase in monomer density around the particles, increasing the level of short-range repulsion. We notice that the potential is shallower for a larger number of chains. To summarize, many-chain simulations seem to be more realistic, as some essential physics of the two-particle system is captured. They also predict the experimentally verified short-range repulsion. This leads us to believe that the experimental structure factor describing micellar or droplet correlations, which has been measured by several groups,[7,18,19] can be reproduced in future work. As a first step, however, the emergence of short-range repulsions needs to be characterized and understood, if we wish to find a more than semiquantitative agreement.[18]

4. Concluding Remarks

We have presented a Monte Carlo study of the configurations of telechelic polymers between two particles. Polymers can either bridge the particles or form loops, and we have connected the number of bridges and loops to the interparticle potential. The generic shape of the fraction of loops and bridges for both ideal and real chains (Figure 3) as a function of distance shows a maximum close to an interparticle distance comparable to the radius of gyration of the chains ($\beta = 1$). This translates into a minimum of the pair potential at the same position. The depth of the minimum decreases strongly with the size ratio between particle and polymer. The small-range part of the potential does not exhibit any strong repulsion. We have traced back this behavior to the possibilities of lateral escape for the chains compressed between particles, as evidenced in the plots of the monomer density around particles. With regard to the difference between real and ideal chains, the potential is deeper for real chains by a factor of approximately five-thirds with a minimum at approximately the same position. The position of the minimum is of course related to the average chain dimensions, to which the distance is normalized. We can only speculate about the reason for the shift in the depth of the potential minimum. It is related to the increase in the number of loops and bridges with respect to the value at infinite separation (Figure 3b). Apparently, the excluded-volume interaction between monomers favors loop formation at intermediate distances, possibly due to a better exploration of the space of swollen chains. The short-range repulsion is even weaker for real chains than for ideal ones, which might be due to a stronger tendency for real chains to avoid the gap between particles. For single chains, all potentials can be normalized such that the minima coincide, and we have given an interpolating function for these master curves in the Appendix.

The absence of repulsive short-range interactions may be due to the small number of polymer chains around the particles. In the case of ideal chains, increasing the number simply increases the potential, as ideal chains do not interact. For real chains, however, we have shown that the crowding of space around particles leads indeed to a short-range repulsion. The dependence of the potential on the interparticle distance is nontrivial, because the minimum shifts to higher β values as the number of chains is increased from 1 to 16. Simultaneously, the depth of the potential becomes less pronounced. In this context, an increase in computational efficiency, e.g., by sampling around known chain configurations, is certainly possible but was not in the scope of this work. With regard to the bias presumably induced by our gradual buildup of the many-chain system, we note that its evaluation is a difficult task, as we wish to avoid the full recalculation of the system after each chain generation failure. The bias is nonetheless expected to be small, due to the rather small monomer volume fractions. Following the suggestion of a reviewer, we have determined the potential for a mean-field many-chain case replacing only one chain at a time, and the result for the potential was found to be consistent with our previous results.

We mention in this context that we have attempted a description of interacting chains with a standard Flory argument for excluded volume. In this case, only ideal chains need to be generated, which is considerably faster. The main characteristics of increasing small-range repulsion, the shift of the minimum toward higher β values, and the weakening of the potential minimum with the number of polymer chains are found. However, the shape of the potential is peculiar, with a plateau between low β and $\beta = 1$, which reflects the distribution of monomers of ideal chains.

For comparison with experiments, it is important to note that we have calculated the pair potential at a fixed number of chains per pair of spheres, rather than at a fixed chemical potential μ of polymer chains, which seems more appropriate due to the reversible thermodynamic character of the droplet association.[18]

Table 1. Positions of Minima of the Pair Potential Function for Ideal Chains for Different Normalized Bead Sizes (α), as a Function of the Normalized Surface-to-Surface Distance (β)

α	U_{min}(ideal)	β_{min}(ideal)
0.50	−0.30079	1.1055
0.75	−0.23164	1.2060
1.00	−0.20270	1.2563
2.00	−0.12887	1.3568
3.00	−0.092435	1.5578
10.0	−0.034085	1.6583

Table 2. Positions of Minima of the Pair Potential Function for Real Chains for Different Normalized Bead Sizes (α), as a Function of the Normalized Surface-to-Surface Distance (β)

α	U_{min}(real)	β_{min}(real)
1.00	−0.32644	0.9942
2.50	−0.15440	1.0233
5.00	−0.081138	1.1403

Such a potential should also improve the description in terms of pair potentials, as equilibration between many-chain situations is automatically included. For ideal chains, the transformation from a Q potential to a μ potential is straightforward using a Legendre transform.[18] For real chains, however, every Q configuration would have to be calculated.

In this article, we have studied the potential between pairs of colloidal particles. In light of these results, one may question if a description in terms of pairs is valid. Indeed, polymer chains have been found to escape from the space between particles, which is not realistic at finite particle concentrations, where other particles surround the pair. A simulation including many particles would be needed. It is clear that our pair-potential approach cannot be generalized easily, as the pair correlation function between particles is a priori unknown. Fixing a given distribution amounts to setting a pair potential, which is precisely the quantity for which we searched. On the other hand, our results can be used as input for the calculation of pair potentials, using either Monte Carlo simulations or integral equations.[31]

Acknowledgment. Work conducted in the framework of the Network of Excellence 'Soft Matter Composites: an approach to nanoscale functional materials' supported by the European Commission. This project has also been supported in parts by ANR under contract ANR-06-BLAN-0097 'Tailored Transient Self-Assembled Networks (TSANET)'.

Appendix

Statistical Properties of Isolated Ideal and Real Chains. The radius of gyration (R_g) and the average end-to-end distance (R_e) have been determined for free ideal and excluded volume chains, to validate our chain generation procedure. The values are also used to normalize the particle radius and interparticle distance, which is why they are given here.

For ideal chains, the results are as follows: $R_g^{free} = 0.408bN_{seg}^{0.5002}$ and $R_e^{free} = 0.999bN_{seg}^{0.5002}$ (the segment length b being set to unity for all other calculations reported in this paper). The exponent is very close to the expected $^1/_2$, and the ratio is close to $\sqrt{6}$.

For excluded volume, we find the following: $R_g^{free} = 0.418bN_{seg}^{0.596}$ and $R_e^{free} = 1.049bN_{seg}^{0.596}$. The exponent is reasonably close to the literature value of 0.588,[30] and the ratio of $\chi = 6(R_g^{free})^2/(R_e^{free})^2 = 0.953$ corresponds to the value given by Des Cloizeaux[32] ($\chi_{DesCloizeaux} = 0.952$).

Master Curves for Pair Potential. The master curves [$y(x) = U/U_{min}$, $x = \beta/\beta_{min}$) of the pair potential for ideal and (single) excluded-volume chains have been fitted empirically by the following functions. For ideal chains, $y = (0.0235x^4 - 1.385x^3 + 1.507x^2 - 0.71861x + 1076)\exp(-0.7369x^2)$. For real chains, $y = (-0.071805x^4 + 0.37157x^3 - 0.46931x^2 - 0.71861x - 0.44603)\exp(-0.28919x^2)$.

The values for U_{min} and β_{min} at each α are given in Tables 1 and 2.

Supporting Information Available: Average monomer density, $\phi(x,z)$, of ideal polymer chains having both stickers attached to a bead. This material is available free of charge via the Internet at http://pubs.acs.org.

References and Notes

(1) Zilman, A.; Tlusty, T.; Safran, S. A. Entropic networks in colloidal, polymeric and amphiphilic systems. *J. Phys.: Condens. Matter* **2003**, *15* (1), S57–S64.
(2) Semenov, A. N.; Joanny, J. F.; Khokhlov, A. R. Associating Polymers: Equilibrium and Linear Viscoelasticity. *Macromolecules* **1995**, *28* (4), 1066–1075.
(3) Annable, T.; Buscall, R.; Ettelaie, R.; Whittlestone, D. The Rheology of Solutions of Associating Polymers: Comparison of Experimental Behavior with Transient Network Theory. *J. Rheol.* **1993**, *37* (4), 695–726.
(4) Lee, J. H.; Gustin, J. P.; Chen, T. H.; Payne, G. F.; Raghavan, S. R. Vesicle-biopolymer gels: Networks of surfactant vesicles connected by associating biopolymers. *Langmuir* **2005**, *21* (1), 26–33.
(5) Zhu, C.; Lee, J. H.; Raghavan, S. R.; Payne, G. F. Bioinspired vesicle restraint and mobilization using a biopolymer scaffold. *Langmuir* **2006**, *22* (7), 2951–2955.
(6) Warriner, H. E.; Davidson, P.; Slack, N. L.; Schellhorn, M.; Eiselt, P.; Idziak, S. H. J.; Schmidt, H. W.; Safinya, C. R. Lamellar biogels comprising fluid membranes with a newly synthesized class of polyethylene glycol-surfactants. *J. Chem. Phys.* **1997**, *107* (9), 3707–3722.
(7) Bagger-Jorgensen, H.; Coppola, L.; Thuresson, K.; Olsson, U.; Mortensen, K. Phase behavior, microstructure, and dynamics in a nonionic microemulsion on addition of hydrophobically end-capped poly(ethylene oxide). *Langmuir* **1997**, *13* (16), 4204–4218.
(8) Ramos, L.; Ligoure, C. Structure of a new type of transient network: Entangled wormlike micelles bridged by telechelic polymers. *Macromolecules* **2007**, *40* (4), 1248–1251.
(9) Lodge, T. P.; Taribagil, R.; Yoshida, T.; Hillmyer, M. A. SANS evidence for the cross-linking of wormlike micelles by a model hydrophobically modified polymer. *Macromolecules* **2007**, *40* (13), 4728–4731.
(10) Nakaya-Yaegashi, K.; Ramos, L.; Tabuteau, H.; Ligoure, C. Linear viscoelasticity of entangled wormlike micelles bridged by telechelic polymers. *J. Rheol.* **2008**, *52*, 359–377.
(11) Appell, J.; Porte, G.; Rawiso, M. Interactions between nonionic surfactant micelles introduced by a telechelic polymer. A small angle neutron scattering study. *Langmuir* **1998**, *14* (16), 4409–4414.
(12) Gradzielski, M.; Rauscher, A.; Hoffmann, H. Hydrophobically Cross-Linked Micellar Solutions: Microstructure and Properties of the Solutions. *J. Phys. IV* **1993**, *3* (C1), 65–79.
(13) Odenwald, M.; Eicke, H. F.; Meier, W. Transient Networks by Aba Triblock Copolymers and Microemulsions: A Rheological Study. *Macromolecules* **1995**, *28* (14), 5069–5074.
(14) Filali, M.; Ouazzani, M. J.; Michel, E.; Aznar, R.; Porte, G.; Appell, J. Robust phase behavior of model transient networks. *J. Phys. Chem. B* **2001**, *105* (43), 10528–10535.
(15) Tanaka, F.; Edwards, S. F. Viscoelastic Properties of Physically Cross-Linked Networks: Transient Network Theory. *Macromolecules* **1992**, *25* (5), 1516–1523.
(16) Zilman, A.; Kieffer, J.; Molino, F.; Porte, G.; Safran, S. A. Entropic phase separation in polymer-microemulsion networks. *Phys. Rev. Lett.* **2003**, *91* (1), 015901.
(17) Hurtado, P. I.; Berthier, L.; Kob, W. Heterogeneous diffusion in a reversible gel. *Phys. Rev. Lett.* **2007**, *98* (13), 000
(18) Porte, G.; Ligoure, C.; Appell, J.; Aznar, R. Bridging interactions due to telechelic linkers balanced by screened Coulombic repulsions. *J. Stat. Mech.: Theory Exp.* **2006**, *05*, 05005.
(19) Puech, N.; Mora, S.; Testard, V.; Porte, G.; Ligoure, C.; Grillo, I.; Phou, T.; Oberdisse, J. Structure and rheological properties of model microemulsion networks filled with nanoparticles. *Eur. Phys. J. E* **2008**, *26*, 13–24.
(20) BaggerJorgensen, H.; Coppola, L.; Thuresson, K.; Olsson, U.; Mortensen, K. Phase behavior, microstructure, and dynamics in a nonionic microemulsion on addition of hydrophobically end-capped poly(ethylene oxide). *Langmuir* **1997**, *13* (16), 4204–4218.

(21) Milner, S. T.; Witten, T. A. Bridging Attraction by Telechelic Polymers. *Macromolecules* **1992**, *25* (20), 5495–5503.
(22) Meng, X. X.; Russel, W. B. Telechelic associative polymers: Interactions between strongly stretched planar adsorbed layers. *Macromolecules* **2003**, *36* (26), 10112–10119.
(23) Eiser, E.; Klein, J.; Witten, T. A.; Fetters, L. J. Shear of telechelic brushes. *Phys. Rev. Lett.* **1999**, *82* (25), 5076–5079.
(24) Dai, L.; Toprakcioglu, C. Forces Between End-Adsorbed Triblock Copolymer Chains and a Bare Mica Surface in a Good Solvent. *Europhys. Lett.* **1991**, *16* (4), 331–335.
(25) Bjorling, M.; Stilbs, P. Using end-confined chains to model end-absorbing, triblock copolymers: 2. Numerical approach. *Macromolecules* **1998**, *31* (25), 9033–9043.
(26) Semenov, A. N.; Joanny, J. F.; Khokhlov, A. R. Associating polymers: Equilibrium and linear viscoelasticity. *Macromolecules* **1995**, *28* (4), 1066–1075.
(27) Bhatia, S. R.; Russel, W. B. End-capped associative polymer chains between nanospheres: Attractions in ideal solutions. *Macromolecules* **2000**, *33* (15), 5713–5720.
(28) Dolan, A. K.; Edwards, S. F. Theory of Stabilization of Colloids by Adsorbed Polymer. *Proc. R. Soc. London, Ser. A* **1974**, *337* (1611), 509–516.
(29) Binder, K., and Paul, W., Recent Developments in Monte Carlo Simulations of Lattice Models for Polymer Systems, *Macromolecules*, **2008**.
(30) Doi, M.; Edwards, S. F. *The Theory of Polymer Dynamics*; Oxford University Press: Oxford, U.K., 1986.
(31) Hansen, J. P.; McDonald, I. R. *Theory of Simple Liquids*; Academic Press: London, 1986.
(32) des Cloizeaux, J.; Jannink, G. *Polymers in Solution*; Clarendon Press: Oxford, U.K., 1990.

MA8005813